PHILOSOPHICAL TRANSACTIONS OF THE ROYAL SOCIETY A MATHEMATICAL, PHYSICAL & ENGINEERING SCIENCES

Wall Effects and Impurities in JET

W. W. Engelhardt

Phil. Trans. R. Soc. Lond. A 1987 **322**, 79-94
doi: 10.1098/rsta.1987.0039

Phil. Trans. R. Soc. Lond. A **322**, 79–94 (1987)
Printed in Great Britain

Wall effects and impurities in JET

By W. W. Engelhardt
JET Joint Undertaking, Abingdon, Oxfordshire, OX14 3EA, U.K.

[Plates 1 and 2]

Impurities in fusion plasmas have two detrimental effects that may render the achievement of ignition difficult: dilution of the reacting plasma reduces the produced fusion power and radiation losses prevent efficient heating up to ignition temperatures. In tokamaks, impurities are released from the containing vessel walls by plasma–wall interaction. They are ionized when entering the plasma and transported into the central plasma by transport processes that are not understood.

The present impurity situation in JET is reviewed in this paper: the main contaminants are carbon, oxygen and nickel, as diagnosed by spectroscopic methods. The concentrations depend on the wall conditioning methods, on the plasma parameters (for example, current and density) and on the power of the applied heating methods. The dilution of hydrogen varies between 20 and 50 % and the total radiation losses range between 30 and 100 %. The central radiation losses are usually small compared with the local heating power. Application of radio-frequency heating in JET does not lead to excessive contamination, in contrast with other experiments.

1. Introduction

One of the main objectives of JET is to study the behaviour of impurities under conditions close to ignition. In fact, without a sufficient purity of the reacting plasma, ignition cannot be achieved. Impurities influence the ignition criterion in two ways.

(i) Any impurity ion of charge Ze expels Z hydrogen ions for a given electron density, if the plasma is to remain quasi-neutral. As the production of fusion power depends on the square of the hydrogen-ion density, this dilution effect can reduce considerably the power production.

(ii) Impurities give rise to electromagnetic radiation by interaction with colliding electrons. This can be bremsstrahlung, recombination radiation or line emission when the impurities are not fully ionized. The maximum ratio between fusion power density and the inevitable hydrogenic bremsstrahlung is 35. Only 1 % of a heavy metal can already make up for this factor. In this case, all fusion power produced is immediately radiated and the combustion cannot sustain itself.

Although a tokamak plasma is isolated from the vessel walls, the confinement of particles is never perfect and particle–surface interactions lead to the release of wall material, which may contaminate the plasma beyond tolerable levels. The physical processes involved are extremely complex. A reliable prediction for fusion-reactor conditions is practically impossible. Only experimental investigations can give the necessary information on the production and distribution of impurities and their effects on the plasma conditions.

This paper highlights the impurity investigations carried out on JET so far. More detailed information on this subject can be found in Behringer *et al.* (1986*a*, *b*), Denne *et al.* (1985) and Engelhardt (1986).

2. General behaviour of impurities in tokamaks

The topology of a tokamak plasma is determined by the magnetic field configuration, which is characterized by nested toroidal surfaces of constant magnetic flux. The plasma pressure is constant on these surfaces with a gradient between them. Particles can diffuse across these surfaces hitting the vessel wall or any protruding material limitation. As the plasma flow along field lines is very rapid, even a poloidally and toroidally localized limiter intercepts practically all particles escaping from the plasma. These have enough energy either to sputter or to evaporate particles from the limiter surface. Also, chemical processes may be involved in the release of material. Neutral impurity atoms with various energies depending on the release mechanism leave the surface, penetrate into the hot plasma where they become ionized and are distributed by cross diffusion in the plasma volume. The resulting impurity concentration depends on the transport mechanism. If a simple Fick's law is applicable, the flux of charged particles is

$$\Gamma_+ = -D\,\partial n_+/\partial r. \tag{1}$$

The charged-particle gradient is building up over the ionization length of the neutral atoms

$$\lambda_{\mathrm{ion}} = v_0/n_e S, \tag{2}$$

where v_0 is the velocity of the neutrals and $n_e S$ their ionization rate due to electron collisions. In steady state, the charged flux Γ_+ and the neutral flux Γ_0 must balance, leading to the simple result

$$\Delta n_+ = \Gamma_0 \lambda_{\mathrm{ion}}/D. \tag{3}$$

Δn_+ may be identified with the impurity density in the plasma, if n_+ at the boundary is zero. For localized limiters, this is not so as the particle density reaches out into the limiter shadow with an exponential decay of the scrape-off layer length, λ_{SOL}. Adding the boundary value, the approximate result is

$$n_+ = (\Gamma_0/D)\,(\lambda_{\mathrm{ion}} + \lambda_{\mathrm{SOL}}). \tag{4}$$

The flux Γ_0 depends on the impinging flux and on the energy of its charged particles. In the simplest case, it is linearly dependent with the sputtering coefficient as a proportionality constant. If the ionization length λ_{ion} is very short, the concentration depends only on the thickness of the scrape-off layer, which depends on the transport processes in the limiter shadow. Sufficient edge temperature is desirable to keep the ionization length small; on the other hand, a compromise must be found to keep the sputtering coefficient, which increases with temperature, sufficiently low. The situation is obviously very involved, keeping in mind that the problem is three dimensional in reality. One-dimensional considerations can only serve as a guideline.

The temperature in the plasma increases monotonically from the edge to the centre. Impurities become multiply ionized successively when they diffuse into the plasma. If transport velocities are not too fast, the distribution among different ionization stages in a tokamak is governed by a balance of ionization and recombination, which depends only on temperature like in the solar corona. 'Corona ionization equilibrium' predicts a shell-like structure of the ionization stages depending on the electron-temperature profile in the plasma. Finite transport velocities tend to displace these shells and to broaden them.

PHILOSOPHICAL TRANSACTIONS OF THE ROYAL SOCIETY A MATHEMATICAL, PHYSICAL & ENGINEERING SCIENCES

The total impurity concentration would be constant in space if (1) holds but, in practice, a more complicated law is expected. In steady state the radial force balance of ions is made up of electric, Lorentz, and kinetic forces

$$Zen_z\,(E_r + U_{pz}\,B_t) = \partial p_z/\partial r, \tag{5}$$

where Ze is the electric charge of the ions, U_{pz} is their poloidal velocity, and n_z and p_z are their density and pressure. Collisions between ions of different Z tend to prevent relative poloidal velocities, which leads to the result

$$\frac{1}{Z_1 n_{z_1}}\frac{\partial p_{z_1}}{\partial r} = \frac{1}{Z_2 n_{z_2}}\frac{\partial p_{z_2}}{\partial r}. \tag{6}$$

Therefore, high Z impurities have steeper relative pressure gradients than hydrogen with $Z = 1$. This effect is also called impurity accumulation and may lead to substantially higher impurity concentrations in the plasma centre.

The understanding of particle transport in a magnetically confined plasma is practically non-existent. Phenomenological descriptions have been given and suggest that there is a common 'anomalous' diffusion coefficient $D \approx 1\ \mathrm{m^2\ s^{-1}}$ for all particles. In addition, there seems to be a convective inward transport with a velocity of order $V_D \sim D/a$, where a is the minor radius of the tokamak. As a result, particle densities are more or less peaked even in the absence of internal sources. However, demixing processes, as described in (6), do occur.

The radiation produced by impurities depends on their number of bound electrons, i.e. their ionization stage. Fully ionized impurities emit only bremsstrahlung that is enhanced over hydrogenic bremsstrahlung by the effective ion charge of a plasma

$$Z_{\mathrm{eff}} = \Sigma n_z Z^2/\Sigma n_z Z. \tag{7}$$

Line emission from partly ionized impurities does not follow a simple law, but depends on the atomic configuration. The general trend is that incompletely filled electronic shells give rise to higher emission. The radiation per ion decreases therefore, whenever a noble-gas-like configuration is reached. With increasing temperature, the radiation per ion decreases in steps until it reaches the final bremsstrahlung level. The dependence on the nuclear charge is approximately quadratic, suggesting that heavy impurities should be avoided in a tokamak. These general trends explain why the total radiation emission profile is usually hollow. Light impurities like oxygen or carbon are fully ionized in the hot plasma centre and radiate mainly in an outer zone. In cases where there is an abundance of heavy impurities like metals, radiation from the centre may be appreciable.

The existence of a 'radiating mantle' can have a positive effect. Power produced or injected into the plasma is uniformly radiated to the walls from an outer region leaving the edge region cold and preventing thereby an excessive impurity production due to charged particles hitting the limiter. On the other hand, a radiative collapse may occur because of an offset of the local power balance. In addition, a cold edge can lead to a redistribution of the current density that may result in a magnetic instability terminating the plasma current. To avoid this effect the electron density at the edge must be kept sufficiently low as radiation increases with density. In fact, impurities play a major role in limiting the electron density achievable in a tokamak.

PHILOSOPHICAL TRANSACTIONS OF THE ROYAL SOCIETY A MATHEMATICAL, PHYSICAL & ENGINEERING SCIENCES

3. Impurity control

Several measures can be taken to reduce the impurity concentrations in a plasma. Wall and limiter materials must be selected to fulfil certain properties, the most important of which are:

low Z number;
low sputtering coefficient;
low susceptibility to chemical reactions;
high melting point, low evaporation rate;
low hydrogen retention;
large thermal conductivity;
resistance against thermal shock.

There is no material that is suited in all respects. JET has chosen to use Inconel as the basic wall material. In some sensitive areas, the wall is covered with carbon tiles. The limiters consist of carbon, at present, but beryllium is being considered as an alternative choice. The walls and limiters must be cleaned after installation and vacuum pump down. This means that volatile contaminants like oxygen, water hydrocarbons are removed by baking to 300 °C and by running low-power glow discharges for many hours. The cleaning discharges are sometimes seeded with methane, to cover the metallic surfaces with a layer of deposited carbon.

From the previous discussion, it is clear that high electron densities lead to a better screening of the incoming impurity flux. At the same time the edge temperature decreases, resulting in a lower production of, at least, some impurities. Therefore, it is advantageous to operate a tokamak at high densities, which in any case, are being aimed at to approach the ignition criterion.

There is a fundamentally different approach to control impurities. The flux of charged particles can be magnetically diverted into a separate chamber where the plasma–wall interaction takes place without affecting the plasma directly. This requires extra coils which are not built into the JET device. It will, however, be possible to create a similar configuration in JET, an open divertor, which may help to control the impurities.

4. Impurity investigations in JET

(*a*) *Measurements*

JET is equipped with powerful impurity diagnostic systems. These have been dealt with by Stott (this symposium). For the scope of this discussion it may be worthwhile to mention the relevant methods briefly.

To monitor the status of the wall, long-term samples are placed in the torus, removed during a shutdown and analysed. Probes can also be exposed during a shot and analysed immediately afterwards. This method allows studies of the effects of wall erosion and deposition. The parameters of the scrape-off plasma are very important to assess the impurity production and screening. These are measured by inserting Langmuir probes into the limiter shadow.

Visible spectroscopy is widely used to determine the location and the amount of impurity influxes. The measurement is based on atomic models relating the emission of a photon to the probability of an ionization process occurring. In the same way the neutral hydrogen influx (which must be equal to the ion outflux in steady state) is determined. The ratio of the impurity

influx to the hydrogen flux gives an experimental impurity release coefficient, which sometimes can be identified with a sputtering coefficient.

Various spectroscopic instruments, that operate from the visible to X-ray regions, are used to observe line emission from the impurity ions in the plasma interior. The wide spectral range is necessary as the photon energy is generally of the same order as the mean electron energy, which varies from a few electronvolts to several kiloelectronvolts. Both survey capability and scanning facility to obtain spatial profiles are available.

Fully stripped ions are normally not accessible by these methods as they do not emit lines. In the presence of heating beams, however, they are excited by charge exchange recombination and can then be observed by visible spectroscopy.

The effective charge number, Z_{eff}, is deduced from a spatially resolved measurement of the bremsstrahlung emission in the visible. The total radiation emission integrated between 6 eV and 10 keV is measured by arrays of bolometers.

The interpretation of all these measurements requires numerical transport simulations to connect single observations on individual ionization stages to a consistent picture. A prerequisite for this is a sufficiently correct phenomenological description of the particle transport, which cannot be provided by theory at present. It is important to check on the consistency of the applied model, wherever it is possible. A further prerequisite is the availability of other diagnostic data on plasma parameters like electron density and temperature.

(*b*) *Results*

(i) *Wall and limiter conditions*

Figure 1, plate 1, shows a photograph of the JET vessel. The inboard wall is covered with carbon tiles to protect the Inconel wall against melting during disruptions, when the plasma moves rapidly inwards. On the left-hand side, a carbon limiter is visible. The plasma is in contact with eight of these limiters, which carry the heat lost to them by conduction. On the right-hand side, two radio-frequency antennas can be seen. The Inconel screen is protected by a carbon-tile picture frame, which is set outwards by a few centimetres with respect to the limiter radius. The main plasma–wall interaction is with the carbon limiters. Figure 2 shows a distribution of various metals across a limiter, analysed after a long period of operation. The relative concentration profile is about the same for all metals, indicating an equilibrium state, where material is eroded in the centre and deposited at the edge of the limiter. This general feature is also seen on the deuterium distribution, where it is even more pronounced. The limiters were installed clean, but heavy interactions of the plasma with the Inconel wall have resulted in a migration of the metals. As the level of absolute concentrations is about the same after different periods of operation, the limiters seem to be in some equilibrium with the wall. During start-up and ramp-down of the current, the magnetic configuration connects the limiter surface with portions of the inner wall. Long-term carbon samples attached to the inner wall and marked with ^{13}C showed a strong ablation to a depth of 400 nm, suggesting that the plasma is eroding the inner wall and probably depositing the material at the limiters and/or the outer wall.

The interception of particles and energy at the limiters leads to a typical interaction zone of a few centimetres. Its projection along the limiter surface determines the power load per limiter area. It is important to know the parameters of this scrape-off layer as they influence

PHILOSOPHICAL TRANSACTIONS OF THE ROYAL SOCIETY A MATHEMATICAL, PHYSICAL & ENGINEERING SCIENCES

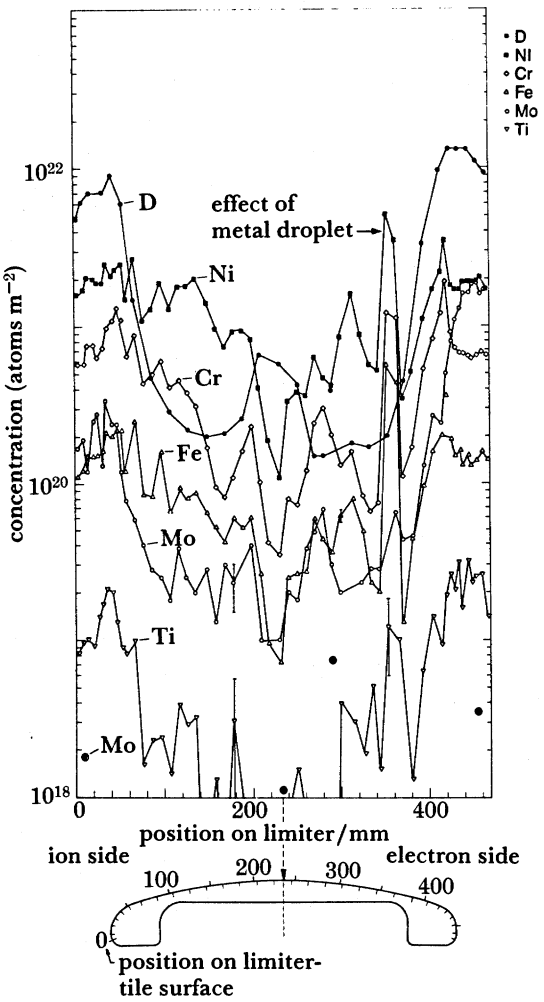

FIGURE 2. Distribution of metal and deuterium concentrations over a JET limiter carbon tile (tile 4, 1984) in the toroidal direction.

both the production and the penetration into the plasma of the impurities. A typical result for decay lengths of power, electron temperature and density is given in figure 3. It is expected that this length is determined by a balance of diffusion velocity perpendicular to the field and plasma flow along the field. Equating the relevant times $\tau_\perp = \lambda^2/D$ and $\tau_\parallel = L/v$, yields

$$\lambda = \sqrt{(DL/v)}. \tag{8}$$

Inserting a typical anomalous diffusion coefficient, D, an appropriate 'connection length', L, and a thermal speed, v, gives a scrape-off thickness, λ, of a few centimetres.

(ii) *Impurity influxes*

The best way to localize and to quantify the impurity influxes is by visible spectroscopy. Figure 4, plate 2, shows a spectrum, where a limiter was partly imaged on the entrance slit of the spectrograph. Lines from neutral atoms are only seen at the limiter surface, whereas lines from charged ions, which leave the limiter following the magnetic field lines, fill the whole length of the slit. Very low ionization stages are still relatively localized and the measurement of their

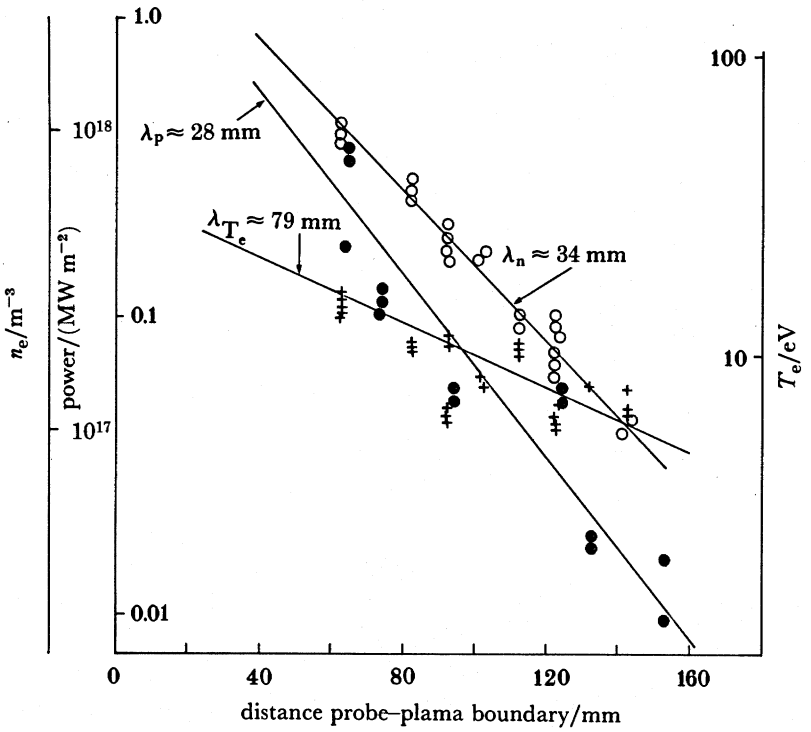

FIGURE 3. Electron temperature, electron density, power density in the scrape-off layer. Conditions $I_p = 2.7$ MA, $B_T = 3.0$ T, $\int n_e \, dl = 5.5$–8.5×10^{19} m^{-2}. Edge values: $n_e = 6.4 \times 10^{18}$ m^{-3}, $T_e = 35$ eV, $P = 2.5$ MW m^{-2}.

absolute intensity together with an appropriate excitation model allows a quantification of the influxes. As the intensity of the hydrogen lines gives also a measure of the plasma flux impinging on the limiter an experimental release rate of impurities can be determined. It is of the order of several percent for carbon and oxygen. For metals it decreases strongly with increasing electron density indicating a cooling of the plasma edge with a consequent reduced sputtering rate. As light impurity influxes increase along with the hydrogen flux (figure 5), it is possible that chemical processes with low interaction energies are involved in their production.

From flux measurements, it became evident that the main sources for metals are the carbon limiters and the metal screens of the antennas. Carbon originates from the limiters and the antenna frame, with a minor contribution from the wall. Oxygen is originating from both wall and limiters. The measurements indicate, however, that there must be areas emitting oxygen in the vessel that have not been looked at yet.

(iii) Impurity concentrations in the plasma

Survey spectra in the wavelength range 100–1000 Å† are shown in figure 6*a*, *b*. The prominent lines come from various ionization stages of oxygen, carbon and chlorine. Spectrum 6*a* is taken at low density with clean walls and displays a number of nickel and chromium lines. Spectrum 6*b* has been obtained after carbonization at higher electron density. The metal lines have nearly disappeared both because of the wall coverage with carbon and because of lower metal influxes at high density.

† 1 Å = 10^{-10} m = 10^{-1} nm.

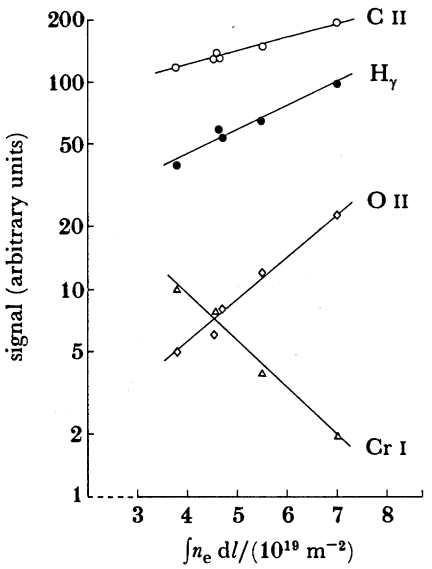

FIGURE 5. Line intensities indicative for particle fluxes measured at the limiter and plotted against plasma density. $I_p = 2$ MA.

The interpretation of these spectra in terms of impurity concentration is not straightforward. Figure 7 shows a calculated distribution of ionization stages over the plasma radius. In the limit of negligible transport, the corona distribution is obtained which deviates considerably from the case where finite transport is included. This is particularly true for the outer plasma zone. The position, the maximum and the width of a shell, must be known to relate the observed line intensities with the concentration. An anomalous diffusion coefficient of $D = 1\ m^2\ s^{-1}$ has been chosen in the example shown. This value is approximately that obtained from other tokamaks, but it must be confirmed if it holds also in a device of the size of JET.

Figure 8 gives a comparison between a measured emission profile of Ni XVII and calculation. Also shown is the profile expected from a corona distribution. The agreement between experiment and calculation is sufficiently good to justify the chosen value for D. In some instances, pieces of nickel fell into the plasma, causing a transient perturbation of the nickel concentration. This event can also be simulated numerically and compared with the time behaviour of the line emission. Figure 9 shows an example giving a very good indication of the value of the diffusion coefficient.

Detailed analysis of many discharges results in typical impurity concentrations as given in table 1. The dominant impurities are carbon and oxygen (*ca.* a few percent), metals are less than 0.1 % and depend more strongly on the plasma conditions and on the history of the vessel. Figure 10 shows line intensities for plasmas with about the same electron density plotted against the discharge number, after a venting of the vessel and installation of clean carbon limiters. Oxygen has a tendency to decrease steadily, carbon stays more or less constant. Nickel is very low in the beginning and increases to a saturated value. Between pulse no. 3650 and no. 4186, a number of irregular discharges were performed, which released wall material and led to a substantial increase of the metal level. Flux measurements showed that the sources of nickel were the carbon limiters which were contaminated with metals. Carbonization could reduce this level to the previous value, but after about 20 discharges the effect had disappeared. The

FIGURE 1. Interior of the JET vacuum vessel.

(*Facing p.* 86)

PHILOSOPHICAL TRANSACTIONS OF THE ROYAL SOCIETY A MATHEMATICAL, PHYSICAL & ENGINEERING SCIENCES

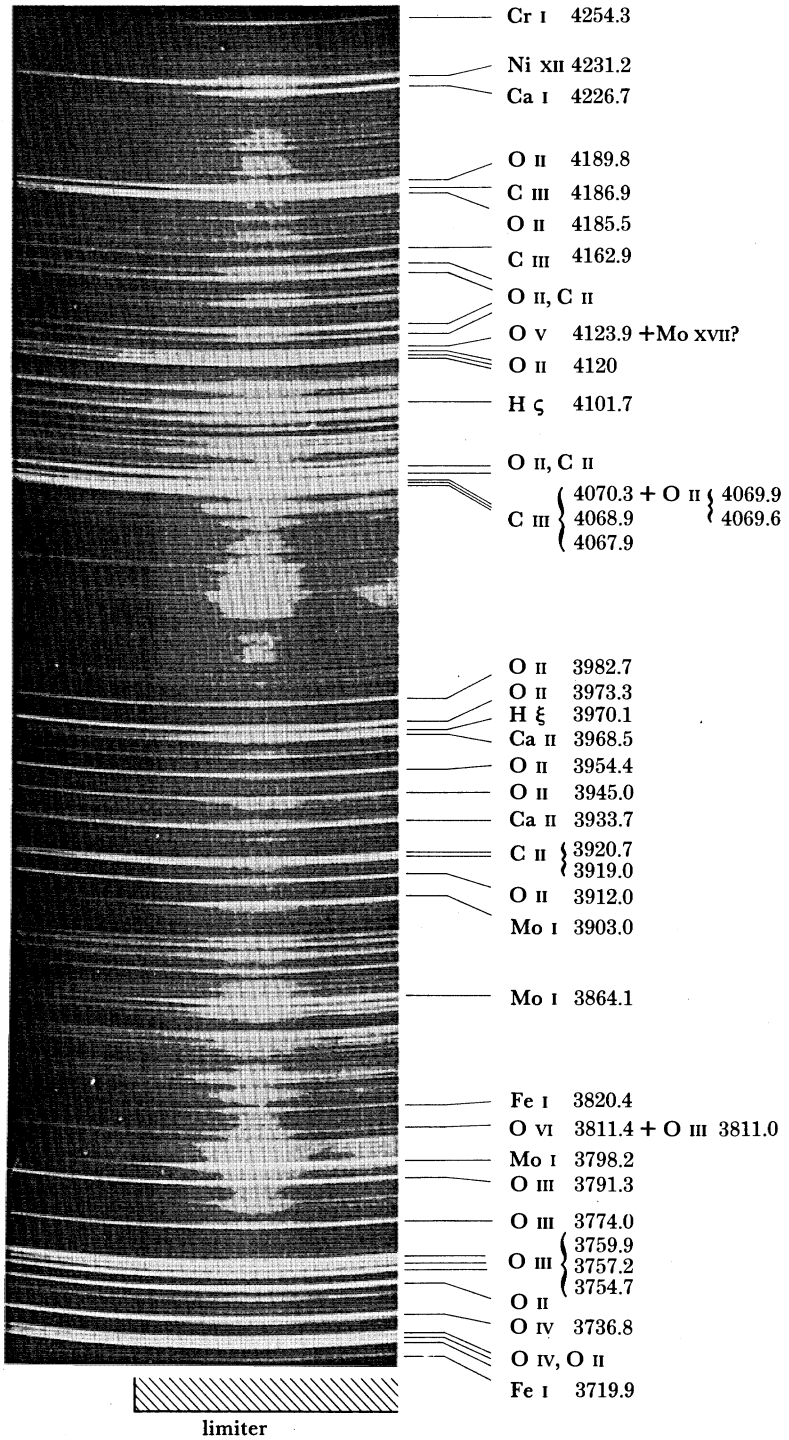

FIGURE 4. Spectrum of impurity lines between 3720 and 4250 Å taken at the limiter (1 Å = 10^{-10} m = 10^{-1} nm).

PHILOSOPHICAL TRANSACTIONS OF THE ROYAL SOCIETY A MATHEMATICAL, PHYSICAL & ENGINEERING SCIENCES

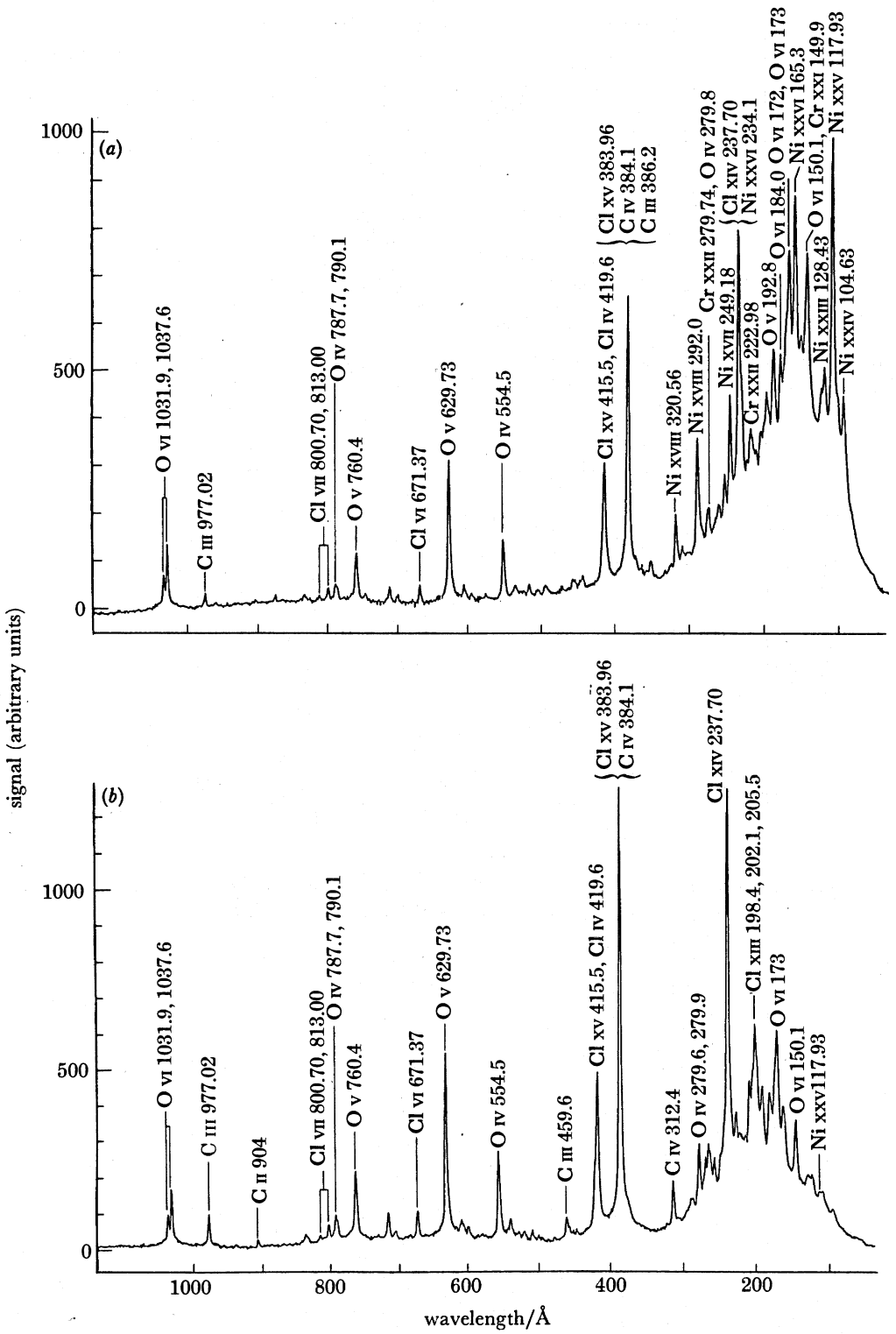

FIGURE 6. Survey spectrum of the JET plasma in the vacuum–ultraviolet region (VUV): (*a*) before carbonization at low electron density; no 2232, $t = 5.57$ s, $I_p = 2.1$ MA, $B_T = 2.6$ T, $\int n_e \, dl = 5.1 \times 10^{19}$ m^{-2}, $b/a = 1.4$; (*b*) after carbonization at high density; no. 2892, $t = 7.4$ s, $I_p = 2.8$ MA, $B_T = 3.4$ T, $\int n_e \, dl = 9.27 \times 10^{19}$ m^{-2}, $b/a = 1.4$.

PHILOSOPHICAL TRANSACTIONS OF THE ROYAL SOCIETY A MATHEMATICAL, PHYSICAL & ENGINEERING SCIENCES

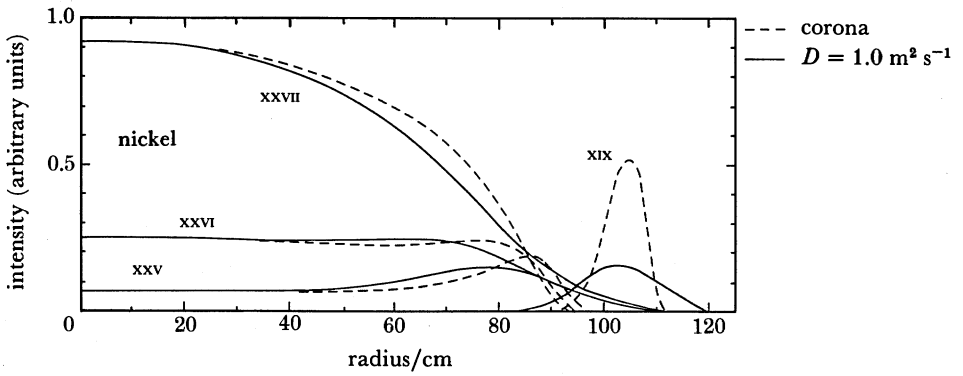

FIGURE 7. Spatial distribution of various ionization stages of nickel calculated for corona equilibrium and for diffusive transport.

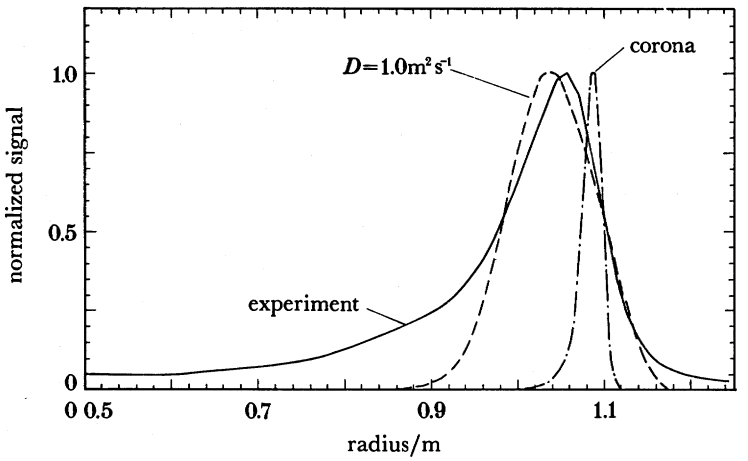

FIGURE 8. Emission profile of a line of Nixvii. Solid line, measured profile; broken lines, corona and finite transport calculation. Nixvii 24.918 nm, $V_D = -2Dr/a^2$.

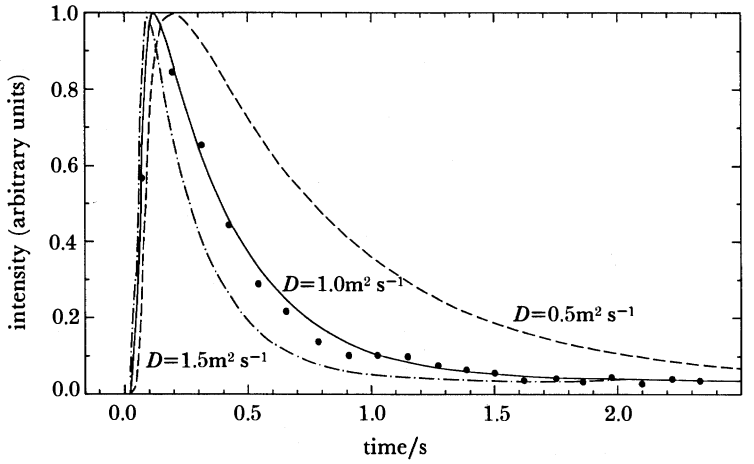

FIGURE 9. Time evolution of a Nixxvi line after injection of a piece of Ni into the plasma. The points are measured, the lines show simulations with various diffusion coefficients. Nixxvi 16.53 nm, $V_D = -2Dr/a^2$.

TABLE 1. MAIN IMPURITIES AND TYPICAL RANGE OF CONCENTRATIONS IN 1985

carbon	2–4 % (of n_e)
oxygen	1–2 %
chlorine	0.05–0.15 %
metals (Ni, Fe, Cr)	0.001–0.3 %

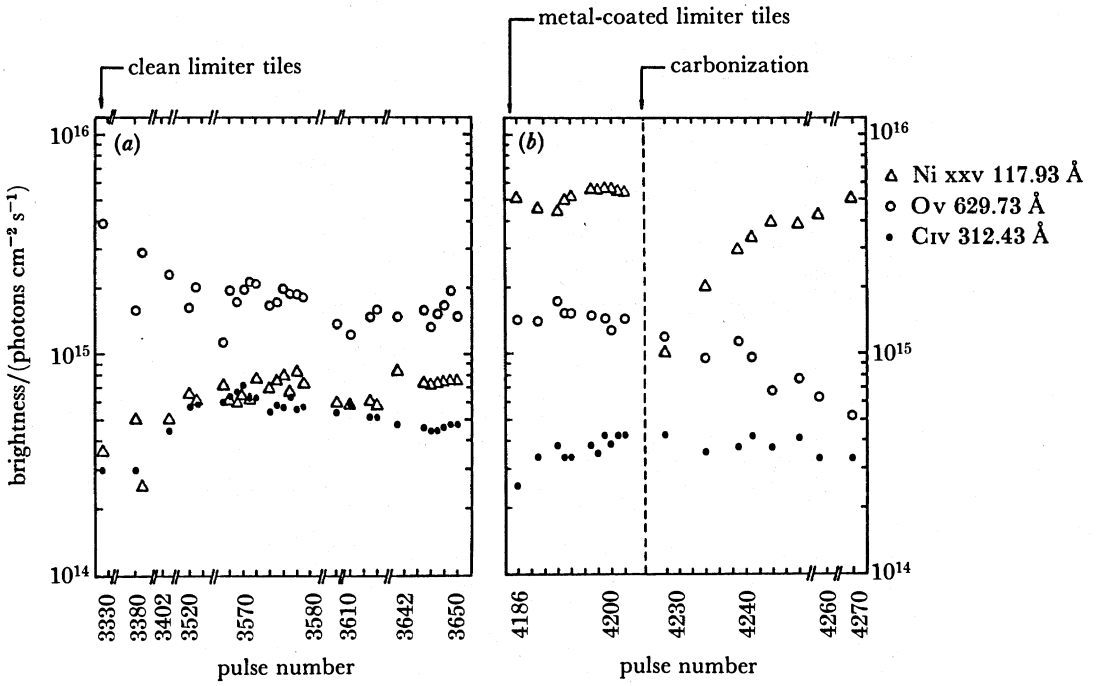

FIGURE 10. Long-term behaviour of impurity lines in JET standard discharges.

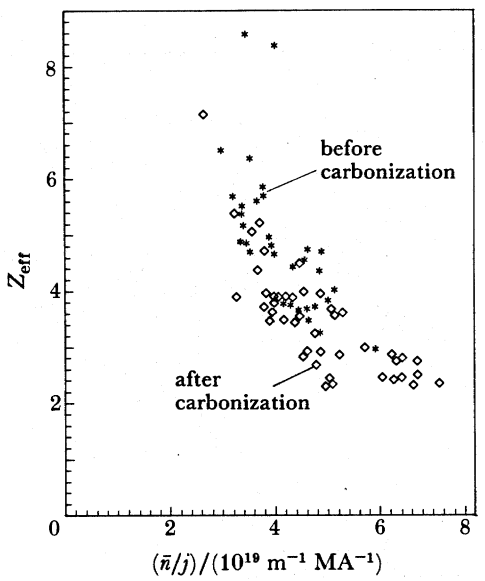

FIGURE 11. Effective charge number (Z_{eff}) plotted against the ratio of average electron density and current density.

PHILOSOPHICAL TRANSACTIONS OF THE ROYAL SOCIETY A MATHEMATICAL, PHYSICAL & ENGINEERING SCIENCES

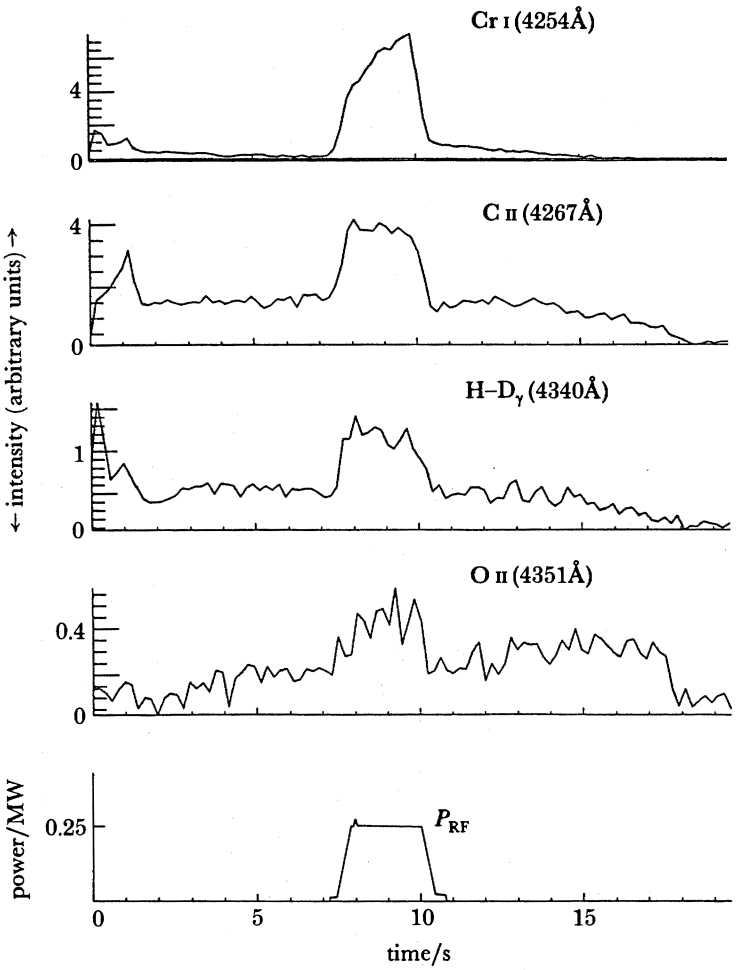

FIGURE 12. Increase of various line intensities emitted in front of an antenna, when RF power is switched on.

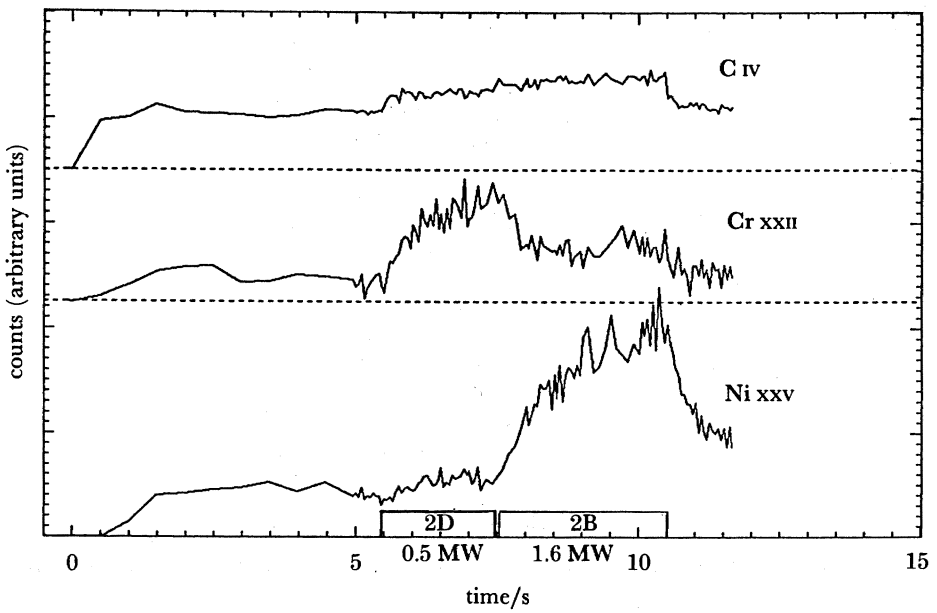

FIGURE 13. Time evolution of chromium and nickel in the plasma, when antennae with different screen material are activated (antenna 2D, Cr; antenna 2B; Ni).

implication is that the metals on the limiter had been covered by a carbon layer which was relatively quickly eroded. At high densities the metal levels are generally very low regardless of carbonization.

The picture emerging from the spectroscopic measurements is reflected in the behaviour of the effective ion charge number. In figure 11, Z_{eff} is plotted against the ratio of electron density and plasma current. The tendency is that the plasma becomes cleaner with increasing density and decreasing current density. Carbonization leads to somewhat better results. It appears to be difficult to reach values below $Z_{\mathrm{eff}} = 2$. The reason is that the light impurity influxes increase with density (figure 5) keeping the relative concentration roughly constant.

(iv) *Impurity behaviour during radio-frequency heating*

When the plasma is heated by RF power the influx of all impurities and that of hydrogen is increased (figure 12). The reason for this behaviour is not clear. It is likely that the transport is enhanced resulting in higher particle losses and consequently stronger plasma–wall interactions. As a result, the electron and the impurity densities increase, but the relative concentrations reflected in the effective ion charge stay approximately constant.

The increase in metal influxes is strongest indicating that they are produced directly at the metallic Faraday screens of the antennas. This becomes evident, when antennas with different screen material are operated. Figure 13 shows the increase of a chromium line and subsequently a nickel line clearly correlated with the activation of two different antennas. Table 2 summarizes the impurity development in a discharge heated by about 3MW RF power. The calculated values of Z_{eff} and of the radiated power refer to spectroscopically determined impurity concentrations and predictions obtained from the impurity transport code.

TABLE 2. CHANGES OF IMPURITY CONCENTRATIONS† DURING A DISCHARGE HEATED BY RADIO-FREQUENCY WAVES

(No. 5414, $B_{\mathrm{T}} = 2.1$ T, $I_{\mathrm{p}} = 2.0$ MA, $P_{\mathrm{RF}} = 2.8$ MW.)

	before RF	during RF
$\bar{n}_{\mathrm{e}}$	1.9×10^{19} m^{-3}	2.3×10^{19} m^{-3}
(C)	1.9%	2.5%
(O)	1.5%	1.2%
(Cl)	0.05%	0.06%
(Ni)	0.005%	0.013%
$Z_{\mathrm{eff}}^{\mathrm{calc}}$	2.58	2.72
$Z_{\mathrm{eff}}^{\mathrm{brems}}$‡	2.71	2.92
$P_{\mathrm{rad}}^{\mathrm{calc}}$	0.80 MW	1.23 MW
$P_{\mathrm{rad}}^{\mathrm{boloms}}$§	0.86 MW	1.46 MW
P_{tot}	1.41 MW	3.81 MW

† Uncertainties in impurity concentrations could amount to ±50%.
‡ Value determined by visible bremsstrahlung.
§ Value determined by bolometric measurements.

(v) *Radiation losses*

The total radiation losses as measured by bolometry range between 40 and 100% of the input power. The low values are obtained at low density with freshly carbonized walls, the 100% value is reached when the density is increased to its limit, where a radiation collapse can occur. Figure 14 shows this behaviour clearly. It is remarkable that the percentage of radiated power

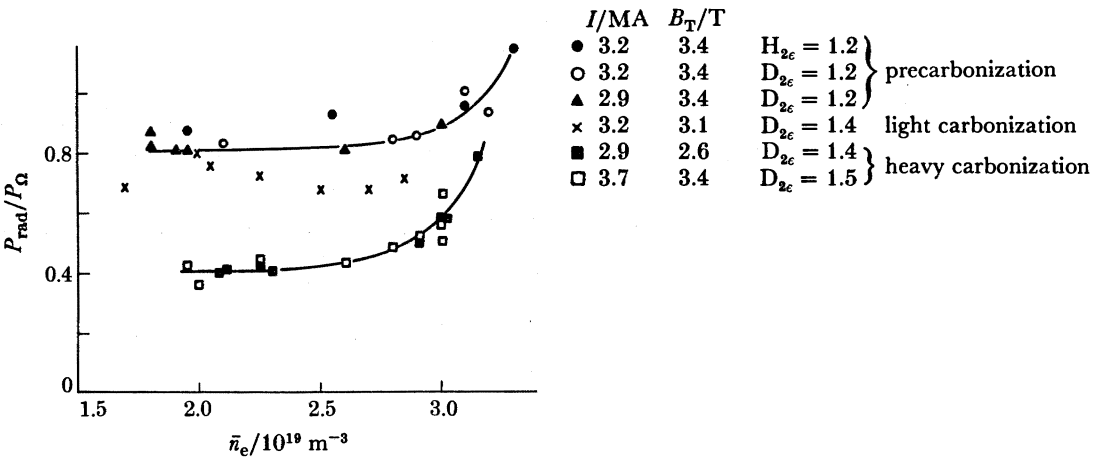

FIGURE 14. The ratio of total radiated power and ohmic input power plotted against electron density for various conditions. $t = 7$ s.

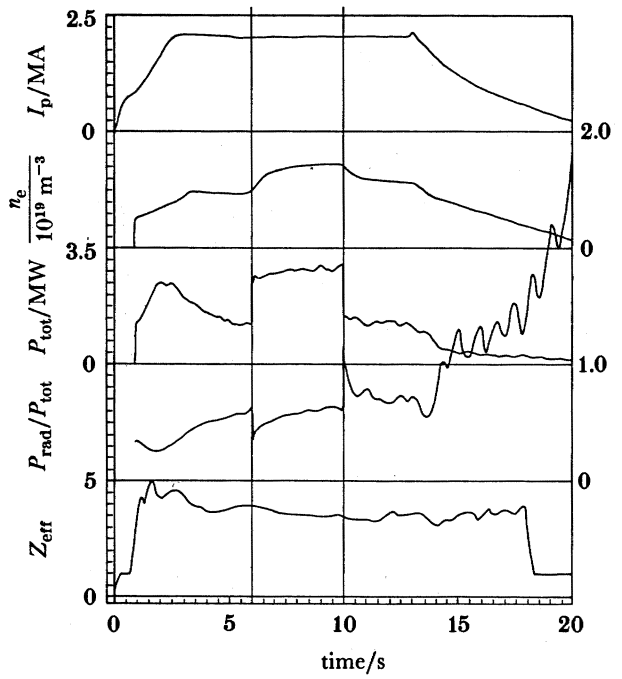

FIGURE 15. Traces of plasma current, electron density, total input power, relative radiated power, Z_{eff} for a discharge heated by RF.

does not change significantly with RF heating. Figure 15 shows a case where the input power is more than doubled, but the radiated portion approaches the same level as in the ohmic phase of the discharge. It is only in very low density discharges that the metal production at the antenna screens leads to a substantial metal concentration in the plasma, accompanied by a higher percentage of radiated power.

Although an appreciable amount of the input power is always radiated, the emission profiles

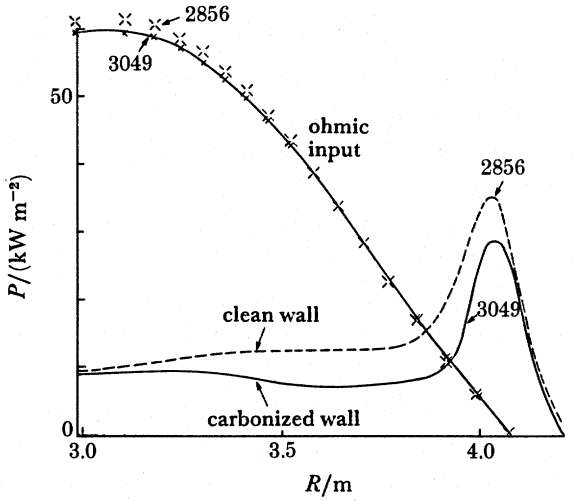

FIGURE 16. Radiation profile as a function of major radius for two discharges before and after carbonization. $I_p = 3.6$ MA, $B_T = 3.4$ T; total radiated power for the clean wall was 2.13 MW and for the carbonized wall was 1.43 MW.

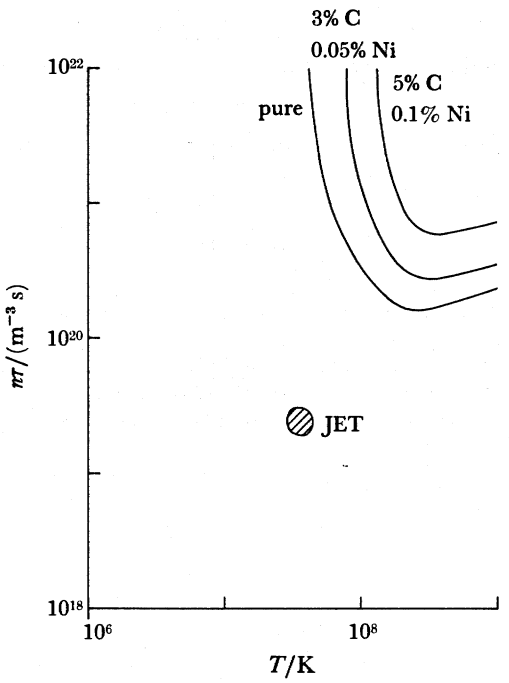

FIGURE 17. Calculated ignition criterion ($n\tau$ against T) for pure and contaminated plasmas. The present parameters for JET are indicated.

of the radiation power densities are generally hollow. This is shown in figure 16, where the ohmic power density is also plotted. For up to two thirds of the plasma radius, the ohmic input substantially exceeds the direct radiation and the heat is lost by transport processes. It is only in an edge zone that radiation takes over and radiates even more than ohmic heating power directly deposited there.

5. Conclusions

It was the purpose of this lecture to show how impurities are produced on the material walls with which the plasma is in contact: how they penetrate the plasma and how they are transported leading to a certain contamination. The main results derived from the investigations on the JET plasma are the following:

the anomalous transport coefficient is of the same order as in other tokamaks;

the concentrations are not excessively high;

catastrophic accumulation of impurities in the plasma centre does not occur;

the impurity radiation losses pose no insuperable difficulty in heating the plasma.

A prediction on the impurity situation when JET approaches thermonuclear conditions is difficult to make. If the present impurity cocktail does not change, the ignition criterion will be altered as shown in figure 17. It is to be expected that higher densities, which have to be achieved anyway, should lead to cleaner plasmas. Additional heating should not have deleterious effects, as the larger amount of power will be removed by more particles at the edge leaving their energy and their capability of producing impurities unaltered. According to what is known so far, JET should not fail to reach its final goal because of impurity problems.

This lecture represents the effort of a large number of people in the JET Team, and of staff from associated laboratories such as Culham Laboratory, U.K. and IPP-Garching, Germany, who collaborated under Task Agreements. The specific contributions of the Spectroscopy and Impurity Physics Group and of the Plasma Boundary Group are gratefully acknowledged.

References

Behringer, K. *et al.*, 1986*a* *Nucl. Fusion* **26**, 751.

Behringer, K. *et al.*, 1986*b* In *Proc. 7th Int. Conf. on Plasma-Surface Interactions in Controlled Fusion Devices, Princeton, 5–9 May 1986.*

Denne, B. *et al.*, 1985 In *Proc. 12th European Conference on Controlled Fusion and Plasma Physics, Budapest, 2–6 September 1985* (ed. G. Grieger) (*Europhysics conference abstracts* **9F**(1), 379.).

Engelhardt, W. 1986 In *Proc. 13th European Conference on Controlled Fusion and Plasma Heating, Schliersee, Germany, 14–18 April 1986* (ed. G. Briffod & M. Kaufmann).

PHILOSOPHICAL TRANSACTIONS OF THE ROYAL SOCIETY A MATHEMATICAL, PHYSICAL & ENGINEERING SCIENCES

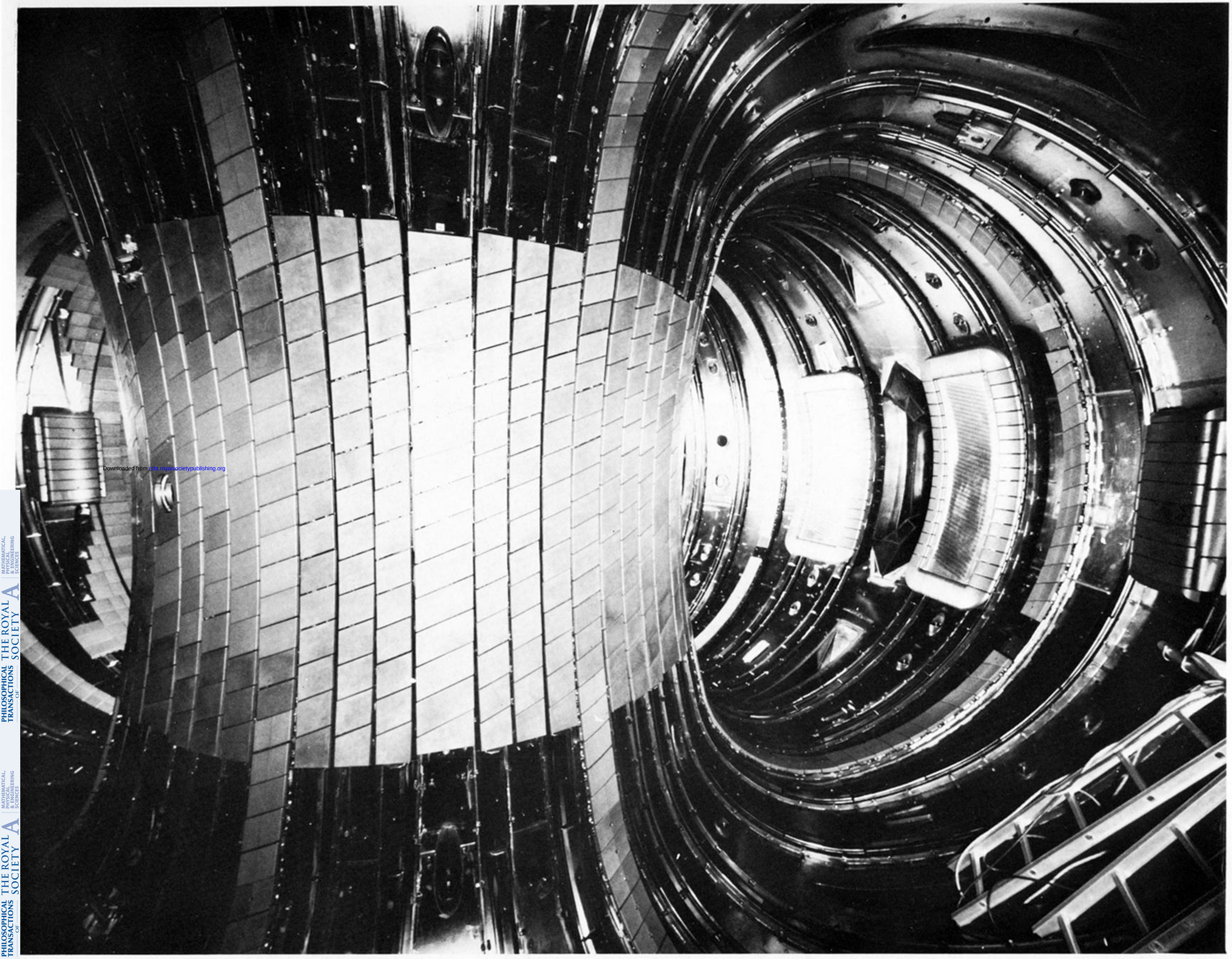

FIGURE 1. Interior of the JET vacuum vessel.

PHILOSOPHICAL TRANSACTIONS OF THE ROYAL SOCIETY A MATHEMATICAL, PHYSICAL & ENGINEERING SCIENCES

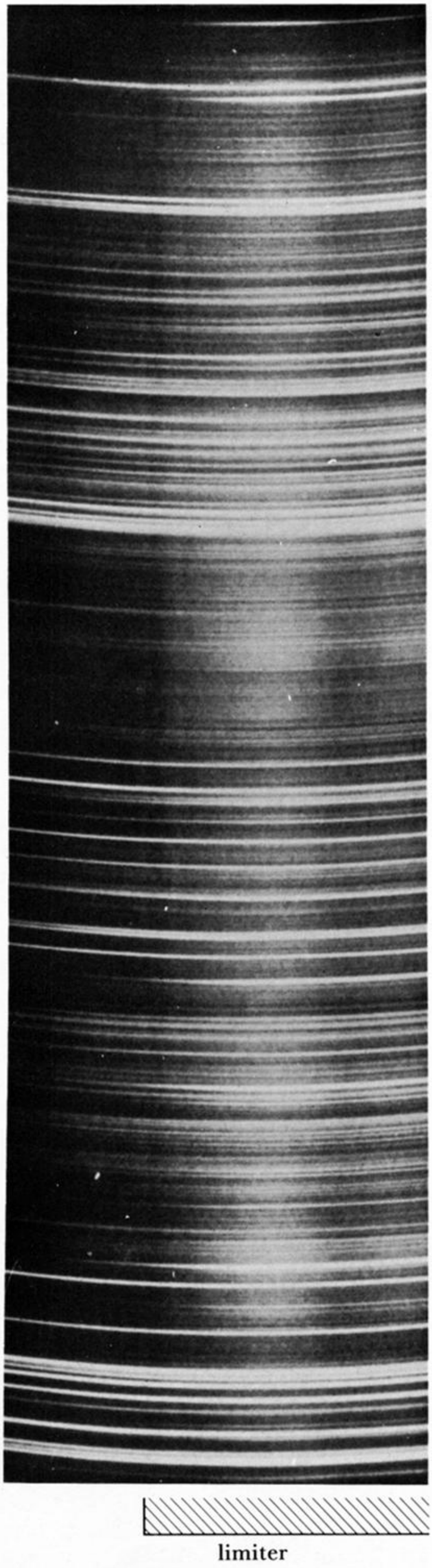

FIGURE 4. Spectrum of impurity lines between 3720 and 4250 Å taken at the limiter (1 Å = 10^{-10} m = 10^{-1} nm).